Acta Geologica Polonica, Vol. 64 (2014), No. 4, pp. 457–472
DOI: 10.2478/agp-2014-0024

Th-U-total Pb timing constraints on the emplacement of the granitoid pluton of Stolpen, Germany

KATARZYNA LISOWIEC[1,2], BARTOSZ BUDZYŃ[3,4], EWA SŁABY[1], BERNHARD SCHULZ[5] AND AXEL D. RENNO[6]

[1] *Institute of Geological Sciences, Polish Academy of Sciences, Warsaw Research Centre, Twarda 51/55, 00-818 Warsaw, Poland, E-mails: klisowiec@twarda.pan.pl, e.slaby@twarda.pan.pl*
[2] *Institute of Geochemistry, Mineralogy and Petrology, University of Warsaw, Żwirki i Wigury 93, 02-089 Warsaw, Poland, E-mail: klisowiec@student.uw.edu.pl*
[3] *Institute of Geological Sciences, Polish Academy of Sciences, Kraków Research Centre, Senacka 1, 31-002 Kraków, Poland, E-mail: ndbudzyn@cyf-kr.edu.pl*
[4] *Institute of Geological Sciences, Jagiellonian University, Oleandry 2a, 30-063 Kraków, Poland*
[5] *Institute of Mineralogy, TU Bergakademie Freiberg, Brennhausgasse 14, D-09596 Freiberg, Germany, E-mail: bernhard.schulz@mineral.tu-freiberg.de*
[5] *Helmholtz-Zentrum Dresden-Rossendorf, Bautzner Landstraße 400, 01328 Dresden, Germany, E-mail: a.renno@hzdr.de*

ABSTRACT:

Lisowiec, K., Budzyń, B., Słaby, E., Schulz, B., and Renno, A.D. 2014. Th-U-total Pb timing constraints on the emplacement of the granitoid pluton of Stolpen, Germany. *Acta Geologica Polonica*, **64** (4), 457–472. Warszawa.

Monazite from the Stolpen monzogranite (SE Germany) was studied to constrain the Th-U-total Pb age of pluton formation. Monazite grains demonstrate subtle to distinct patchy zoning related to slight compositional variations. Textural and compositional characteristics indicate that the monazite formed in a single magmatic event in a slightly heterogeneous system, and was only weakly affected by secondary alteration, which did not disturb the Th-U-Pb system. Chemical dating of the monazite gave a consistent age of 299 ± 1.7 Ma. The current study presents the first geochronological data for the Stolpen granite. It provides evidence that Stolpen is the youngest Variscan granitic intrusion in the Lusatian Granodiorite Complex and indicates that magmatic activity related to post-collisional extension in this region lasted at least 5my longer than previously assumed.

Key words: Monazite, Th-U-Pb chemical dating; Lusatian Granodiorite Complex; Stolpen Granite; Variscan granitoids.

INTRODUCTION

The convergence of Gondwana and Laurassia during the Paleozoic, including subduction and continental collision, produced a wide variety of magmatic and metamorphic rocks from the Bohemian Massif in the east to the Massif Central in the west. Due to intensive heating and melting of the crust and/or the mantle, caused by burial or decompression during late-orogenic extension, many granitic intrusions formed, often deriving their melts from heterogeneous sources (e.g. Finger *et al.* 1997; Finger *et al*. 2009; Siebel *et al*. 2003; Förster and Romer 2010). The granitoid bodies are most abundant in the Moldanubian Zone of the orogenic belt

(the main part of the Bohemian Massif) and less abundant in the Saxo-Thuringian and Teplá-Barrandian zones (e.g. Finger *et al*. 1997; Oberc-Dziedzic *et al*. 2013). They differ in petrography, geochemistry and geochronology (Finger *et al*. 1997); therefore a careful study of all the types is crucial to understanding their evolution and global mantle-crust interactions related to orogenic and post-orogenic movements.

The ages of the Variscan granitoids have been constrained in numerous papers using various methods including the Single Zircon Evaporation method (e.g. Kröner *et al*. 1994; Siebel *et al.* 2003), whole rock Rb-Sr (e.g. Kröner *et al*. 1994; Finger *et al*. 1997), the U-Pb method in zircon and monazite (e.g. Gerdes *et al*. 2003; Klein *et al*. 2008; Finger *et al*. 1997; Oberc-Dziedzic *et al*. 2013; Kryza *et al.* 2012) and Th-U-total Pb of uraninite and Re-Os of molybdenite (Förster *et al*. 2012). All these methods are not interchangeable with each other and may document slightly different stages of the magmatic/metamorphic events. Fluid overprint further complicates the use of some of them, e.g. U-Pb ages of zircon or monazite due to remobilization of Pb.

One of the most rapid and widely used methods of age determination is Th-U-total Pb dating of monazite. Monazite is a LREE-rich phosphate [$(REE,Th,U)PO_4$] which incorporates significant amounts of Ce, La, Sm and Nd, as well as other elements such as Y, Th and U. Thelast two are particularly important in terms of using monazite for Th-U-Pb dating. Because monazite occurs in various types of magmatic, metamorphic and sedimentary rocks, it can be used to constrain the timing of geological processes such as magma crystallization and metamorphism or to define the age of protholith(s) (Williams *et al*. 2007). Diffusion of major and trace elements in monazite is very slow (Cherniak and Pyle 2008; Cherniak *et al*. 2004a; Cherniak *et al.* 2004b; Parrish 1990), therefore it can preserve compositional zoning which records different stages of crystallization or metamorphic deformation. Due to the fact that monazite contains negligible amounts of common Pb relative to radiogenic Pb (Parrish 1990), it is possible to use the chemical Th-U-total Pb method employing an electron microprobe to constrain its age (Jercinovic and Williams 2005; Jercinovic *et al*. 2008; Konečný 2004; Montel *et al.* 1996; Pyle *et al.* 2005; Spear *et al*. 2009; Suzuki and Adachi 1991, 1994; Suzuki and Kato 2008). Although chemical dating of monazite is mostly used in metamorphic petrology (Finger and Krenn 2007; Kohn *et al*. 2005; Liu *et al*. 2007; Rosa-Costa *et al.* 2008; Tickyj *et al.* 2004; Williams *et al*. 2007), it has also found applications in constraining the ages of magmatic events with high precision (Just *et al.* 2011). The resistance of monazite to complete alteration and its ability to preserve its growth textures provide an opportunity to reach deep into the magmatic history.

One region of the Variscan Orogenic Belt where granitic intrusions are rather scarce is the Lusatian Granodiorite Complex (LGC), located in the eastern part of the Saxo-Thuringian Zone. It experienced only minor metamorphism and deformation during the Variscan orogeny (Kröner *et al*. 1994). It contains only several late-Variscan granitoid bodies, most of which have been studied in terms of geochemistry and geochronology (Kröner *et al*. 1994; Hammer *et al*. 1999; Förster *et al*. 2012). However there is one pluton,– the Stolpen granitoid,, which cannot be precisely situated within the intrusion sequence of the Lusatian Block due to a lack of geochronological data. This study reports monazite U-Th-Pb timing constraints on the formation of the Stolpen pluton.. The analyzed monazite formed mostly at the magmatic stages of pluton formation; however, as infiltration by post-magmatic fluids has been already documented (Lisowiec *et al*. 2013), the samples were carefully studied to minimize the influence of fluid-alteration on the calculated ages.

GEOLOGICAL SETTING

The granitoid pluton of Stolpen is located in the southern part of the Lusatian Granodiorite Complex which comprises the central part of the Lusatian Anticlinal Zone at the NE margin of the Bohemian Massif (Text-fig. 1). The pluton is slightly SE-NW elongated, which is the main direction of shearing during the Variscan orogenesis (Krentz in Kozdrój *et al*. 2001). Magma emplacement used tectonic faults that were formed during and after orogenic movements. The pluton intruded Cadomian to Early-Palaeozoic (600–490 Ma) magmatic – tonalitic to syenogranitic in composition, locally metamorphosed rocks. The envelope of the complex consists of upper-Proterozoic sedimentary rocks, mostly greywackes and pelites. The Stolpen granite belongs to the group of late- to post-Variscan intrusions in the Lusatian Granodiorite Complex which contains also the amphibole granites of Wiesa and Grossschweidnitz and the biotite granite of Königshain-Arnsdorf, with ages constrained by zircon-evaporation method at 304 ± 10 Ma, 312 ± 10 Ma and Th-U-total Pb dating of uraninite and molybdenite at 327–328 Ma, respectively (Kröner *et al*. 1994; Förster *et al*. 2012).

Knowledge of the petrogenesis of the Stolpen granite is very limited; however Hammer *et al*. (1999) sug-

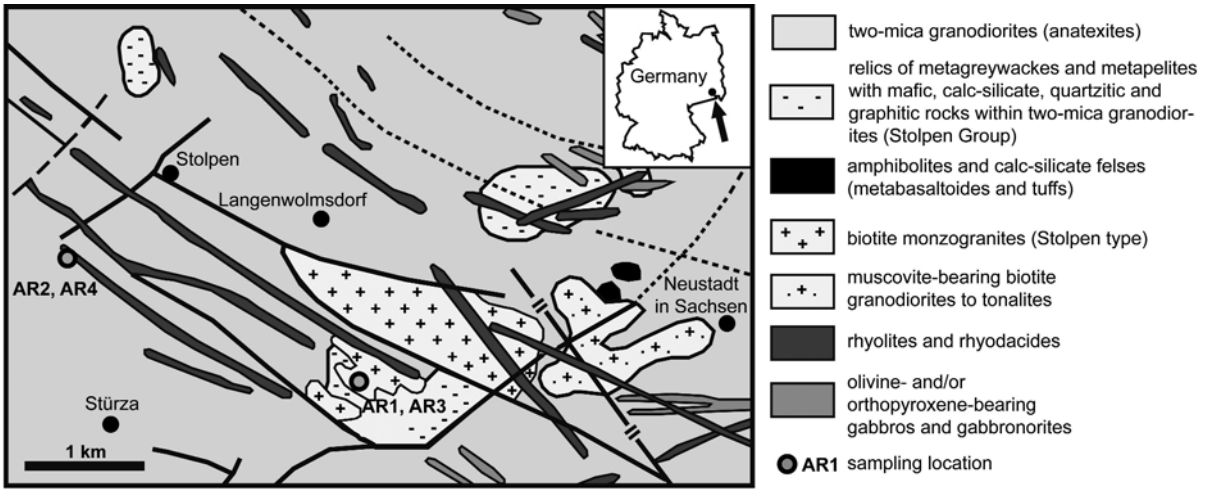

Text-fig. 1. Sketch of the study area (after Kozdrój *et al*. 2001) with sampling locations. AR1, AR3 – 51°0'58.77" N, 14°7'27.71" E

gest that it originated from a crustal magma. The melting process was induced by an upwelling mantle diapir preceded by a fluid front. The fluids were responsible for crustal magma enrichment in LILE and HFSE. An accessory mineral study was consistent with such an hypothesis but did not exclude other possibilities (Lisowiec *et al*. 2013). Hammer *et al*. (1999) place the pluton among other Variscan granitic intrusions but do not give an exact age. It is therefore unknown where exactly it is positioned among other Variscan intrusions in the region.

The pluton consists mostly of medium- to coarse-grained monzogranite of peraluminous character (Hammer *et al.* 1999). Whole-rock geochemistry was documented by Hammer *et al*. (1999) and is presented in Table 1. The authors also report an average Th/U ratio of 4.4. Granite samples used in this study were taken from the SW part of the magmatic body, which consists of a quite homogenous, medium-grained facies. The mineralogy of the granite is quite typical, the main assemblage containing quartz, alkali-feldspar, plagioclase, biotite and small amounts of muscovite. Quartz forms two populations: older large crystals and younger small crystals occurring as inclusions in other minerals or located interstitially. Alkali-feldspar is K-rich with a subordinate Na-rich (anorthoclase) component, whilst the plagioclase composition is almost pure albite, rarely oligoclase (Ab<20%). The pure albitic composition may suggest secondary post-magmatic crystal-fluid interaction. Plagioclase often exhibits weak zonation. Alkali-feldspar shows a strong perthitization and is often replaced by plagioclase (albite) on the margins, which again may be related to reaction with fluids. Similarly the other phases show pristine magmatic compositions affected by interaction with fluids. Biotite underwent almost total chloritization and its FeO content reaches ~43 wt%. Rarely its margins are replaced by muscovite. Accessory minerals present in the granite are fluorite, zircon, monazite (with a high contribution from a cheralite component), titanite, allanite, apatite, xenotime, Y-rich silicates and Y-Ti-phases, Th-rich minerals (oxides and silicates), Nb-Ta minerals (mostly columbite), Fe-oxides and secondary REE-carbonates. Fluorite is the most abundant accessory mineral and forms three populations: homogenous, more or less regularly zoned and patchy. Individual populations show no specific textural positions. Y-rich minerals are represented

Element/ oxide	Content	Element	Content	Element	Content
SiO_2	75.60	Cs	4.5	U	7.8
TiO_2	0.17	Cu	8	V	13
Al_2O_3	13.00	Ga	23	Y	58
Fe_2O_3	1.50	Hf	5.0	Zn	32
MnO	0.03	Li	57	Zr	174
MgO	0.19	Nb	28	La	33
CaO	0.70	Ni	6	Ce	75
Na_2O	3.60	Pb	28	Nd	36
K_2O	4.50	Rb	254	Sm	7.2
P_2O_5	0.05	Sc	4.2	Eu	0.32
Ba	220	Sr	36	Tb	1.30
Co	1.2	Ta	2.56	Yb	3.9
Cr	5	Th	29.6	Lu	0.56

Table 1. Whole-rock chemical composition of the Stolpen monzogranite (from Hammer *et al.* 1999). Element oxides are given in wt [%], trace elements in [ppm].

mostly by strongly zoned hingganite–(Y) and aeschynite–(Y) (Lisowiec *et al*. 2013). Zircon, monazite and xenotime sometimes form intergrowths. The accessory mineral assemblage (mostly zircon and monazite) and the evidence of magmatic and post-magmatic processes that it carries has been studied by Lisowiec *et al*. (2013). Some parts throughout the pluton have more aplitic or pegmatitic character with nearly the same mineral composition as the granite. In the area we can find also numerous andesitic (and one rhyolitic) dykes which are situated in the vicinity of the pluton or intruded within the granite.

ANALYTICAL METHODS

Granite samples were initially crushed in a jaw crusher, than fragmented using a Selfrag high voltage pulse power fragmentation. Afterwards, the two smallest fractions of 500–250 μm and 80–250 μm were used for separation in heavy liquids. The mineral separates were mounted in epoxy and polished.

Backscattered electron (BSE) images were made using a Quanta 600 FEG-MLA600F field emission scanning electron microscope (SEM) equipped with two energy dispersive spectrometers (EDS) at the Institute of Mineralogy, TU Bergakademie Freiberg, Germany. The analytical conditions were as follows: accelerating voltage 20 kV, with some exceptions when 15, 25 or 30 kV were used, and a 200 μA beam current with the beam focused on the sample coated with carbon.

Analyses of Th, U, Pb for the calculation of monazite ages, as well as Y, REE, Ca, Si, P, Sr, Al and As for corrections and evaluation of the mineral chemistry, were carried out using a Cameca SX-100 electron microprobe at the Department of Electron Microanalysis in the State Geological Institute of Dionýz Štúr in Bratislava. The analytical methods for age determination followed procedures presented in Petrik and Konečný (2009). To obtain the optimum c/s/nA (counts per seconds divided by sample current) and to minimize surface damage the following analytical conditions were used: accelerating voltage 15 KV, sample current 180 nA, counting times: Pb of 300 s, Th 35 s, U 80 s, Y 40 s, REE 10–50 s, except Lu 100 s, P, S, Al, Si and Ca 10 s, Sr 20 s, As 120 s. Calibrations were performed using synthetic and natural standards: REE and Y were taken from phosphates XPO_4, Th from ThO_2, Pb from $PbCO_3$, U from UO_2, Ca and Si from wollastonite, As from GaAs, S from barite and Al from Al_2O_3.The resulting ages were calculated using the statistical approach of Montel *et al*. (1996).

RESULTS AND DISCUSSION

Textures and chemical composition of monazite

Monazite is quite abundant in the accessory mineral assemblage of the Stolpen granite (Lisowiec *et al*. 2013). Generally it forms sub- to anhedral 10–20 μm inclusions in fluorite and K-feldspar. It often occurs also in the rock matrix as subhedral crystals up to 300 μm in size. The whole population of monazite grains represents a wide spectrum of growth textures, from nearly homogenous to irregularly zoned, spongy and strongly dissolved (Text-fig. 2), evidence of fluid overprint (Lisowiec *et al*. 2013). The penetrating fluids were enriched in fluorine, Ca, Y and CO_2, based on the high abundance of secondary fluorite and Y-rich silicates. Such a fluid composition enabled the remobilization of trace elements from the monazite grains which were later incorporated into secondary accessory phases. Alterations in monazite include mostly enhanced huttonite and cheralite substitutions. The monazite crystals forming inclusions in fluorite are partly corroded at the contact with the host mineral. Small monazite grains occasionally overgrow zircon margins.

Because of the alteration, careful selection of the grains and evaluation of their chemistry had to be undertaken prior to any chemical dating analysis. Twelve monazite grains, which represent the most 'pure' monazite end-member, were selected for age determination (Text-fig. 3). The monazite grains show very subtle (Text-fig. 3abe) to distinctly patchy zoning (Text-fig. 3dgh). Dark patches in BSE imaging are often located along rims (Text-fig. 3cdghjl). Locations of the spot measurements were chosen carefully to avoid any contribution of potentially fluid-altered domains; therefore,

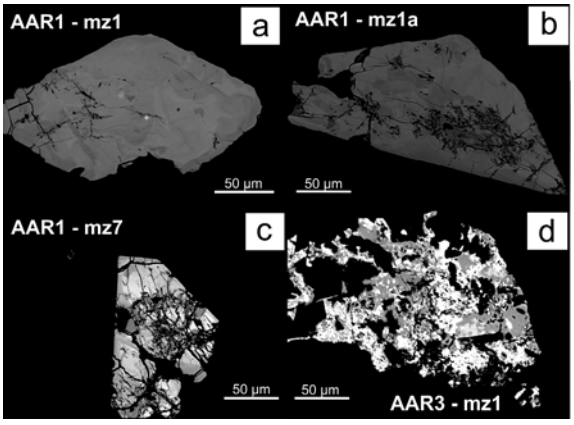

Text-fig. 2. T Representative BSE images of monazite grains and their textures; a – monazite grain with the most homogenous texture showing only very subtle patchy zoning; b, c – monazite grains with more distinct patchy zoning; d – monazite grain with a very strongly resorbed texture

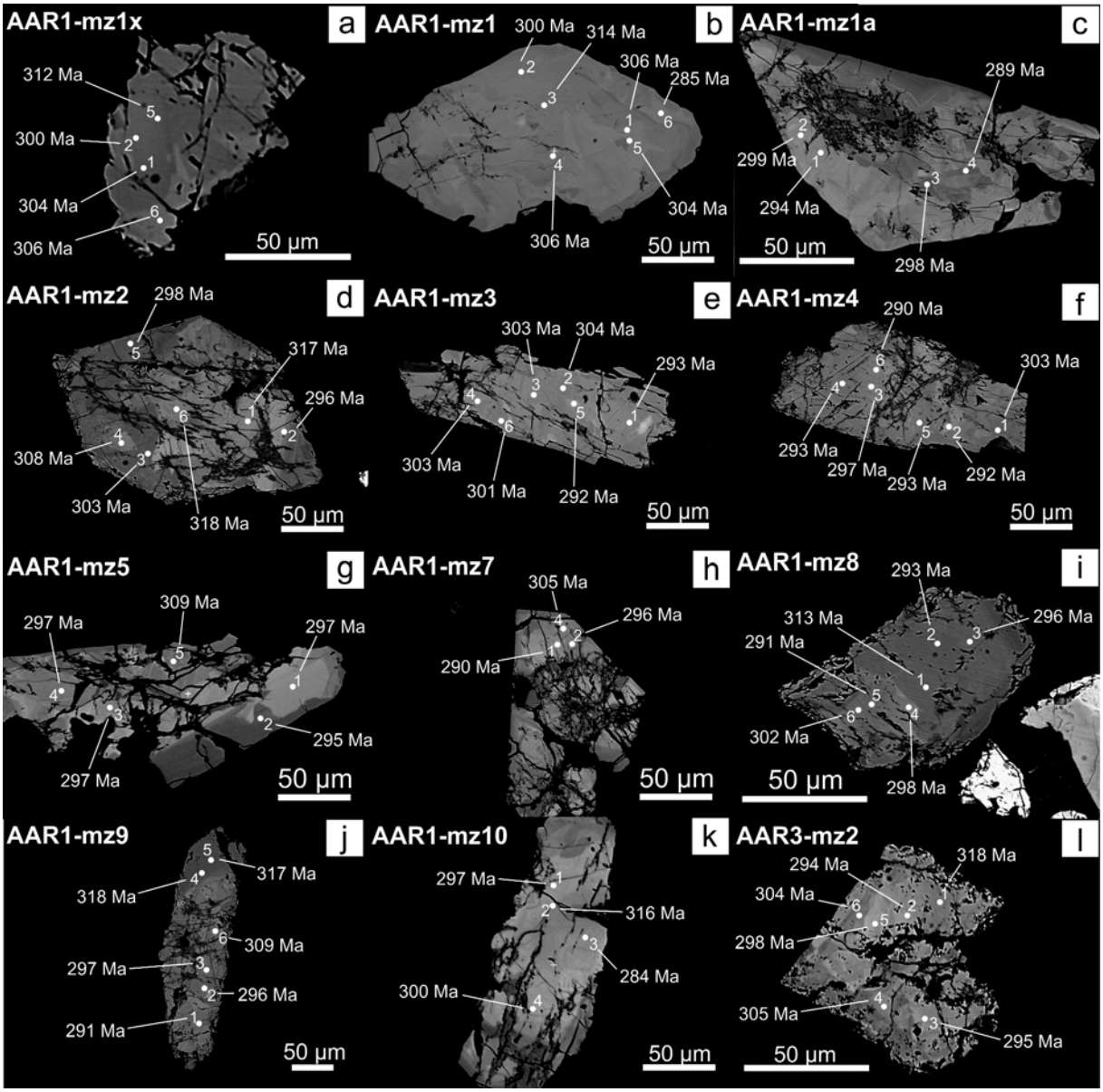

Text-fig. 3. BSE images of twelve analyzed grains with measured points and calculated ages; a, b, e, f and i – grains with subtle patchy zoning and slight variations in chemical composition; c, d, g, h, j, k and l – grains with more distinct patchy zoning and more significant variations in chemical composition; in grains c, d, g, h, j, k, l BSE-dark zones are located on the margins or along cracks

where it was possible, at a safe distance from margins and cracks. However, both types of zones, BSE-bright and BSE-dark, were investigated in order to assess the potential difference in chemical composition and age characteristics, which in some cases meant analyzing small patches close to margins or crevices.

The chemical composition of the entire monazite population shows their affinity to the monazite-huttonite series, with the main substitution mechanism: $Si^{4+} + Th^{4+} (U^{4+}) = REE^{3+} + P^{5+}$ (Text-fig. 4ab). Grains with subtle patchy zoning show only slight differences in element concentrations (AAR1-mz1x, mz1 and mz3 in Table 2). Th, U and Pb contents in a single grain vary in the ranges 3.00 wt.%, 0.30 wt.% and 0.05 wt.%, respectively. Monazite grains showing more distinct zoning demonstrate stronger variations in composition, mostly in Th, U,Pb, Y and La. The highest chemical gradient can be observed in grain AAR1-mz9 where the BSE-dark rim is strongly depleted in Th and Pb (spot 4 and 5); and AAR3-mz2, where the BSE-bright patch

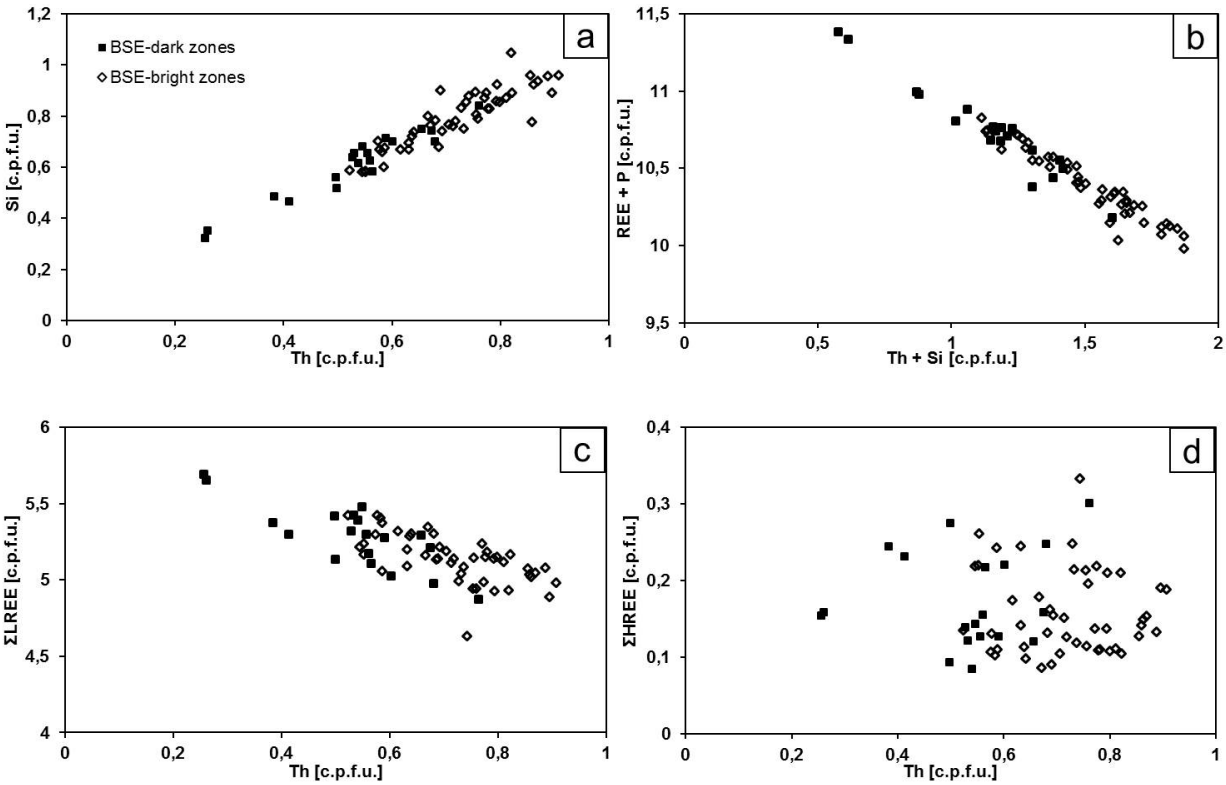

Text-fig. 4. Chemical composition plots of monazite grains; a, b – plots showing the main substitution mechanism in the structure of monazite : $Si^{4+} + Th^{4+} (U^{4+}) = REE^{3+} + P^{5+}$; c – LREE vs. Th plot showing decreasing LREE content with increasing Th abundance; d – HREE vs. Th plot showing no correlation between these elements

(spot 3) is highly enriched in Y, U and HREE, and depleted in LREE. BSE-dark parts of the grains are usually depleted in Th, U and Pb, interpreted as related to decreasing availability of Th and U during monazite growth. Depletion in these elements is coupled with enrichment in LREE. There is no correlation between Th and heavier lanthanides or yttrium (Text-fig. 4cd).

The growth textures along with the chemical composition of monazite grains were studied carefully in terms of primary vs. secondary origin to ensure the quality of the age data. Grains with very subtle patchy zoning and a low chemical gradient are undoubtedly of primary magmatic origin. In cases where the BSE intensity shows more distinct differences between the zones, the possibility of BSE-dark patches (depleted in Th, U and Pb) being altered by secondary hydrothermal processes has to be taken into account. These examples include mainly grains mz2, mz5, mz7 and mz10,where the patchy character is slightly more pronounced. Dark patches are usually associated with crystal margins or cracks. Several measurement points are located on the BSE-dark patches and margins; however their composition does not reveal any significant post-magmatic fluid overprint. These domains are indeed depleted in Th, U and Pb, but the degree of depletion is comparable for all three elements. Such a feature is not likely to take place during fluid alteration which usually results in preferential depletion (or enrichment) in one or two of these components, most usually only Pb (e.g. Williams *et al*. 2011; Harlov *et al*. 2011). The compositional variations, especially the Th-, Pb- and U-contents, can be therefore attributed most probably to fluctuations in melt composition during crystal growth. Binary plots carry further evidence of the negligible contribution of fluid overprint. Th vs. Si diagrams (Text-fig. 4a) are well correlated and almost all points lay within the thin correlation line. Furthermore, points representing both BSE-bright and BSE-dark domains form the same trend on the plots (Text-fig. 4abc). The only distinction of the BSE-bright zones relative to BSE-dark ones is the enrichment in light- and especially heavy-rare earth elements, and Th, U and Pb. Numerous studies have shown that zones affected by post-magmatic fluid alteration display a distinct chemical pattern, distinguishable from the domains formed at the magmatic stage and therefore allowing a straightforward location

Table 2.
Electron microprobe analyses of twelve analyzed grains (wt%).

Sample	AAR1																					
Grain	mz1						mz1a					mz2						mz3					
Point no.	1	2	3	4	5	6	1	2	3	4	5	1	2	3	4	5	6	1	2	3	4	5	6
SO_3	bd	bd	bd	0.028	0.031	0.030	bd	bd	bd	bd	bd	bd	0.030	bd	0.026	bd	bd	0.031	0.033	bd	0.035	bd	bd
P_2O_5	23.761	22.774	23.498	23.684	22.835	23.458	23.164	22.630	23.190	22.990	24.263	24.189	23.459	25.555	24.490	25.793	24.420	23.708	24.022	23.641	24.290	23.484	24.219
As_2O_5	0.272	0.261	0.279	0.273	0.269	0.291	0.274	0.307	0.281	0.284	0.306	0.193	0.285	0.239	0.261	0.260	0.290	0.266	0.286	0.294	0.235	0.310	0.317
SiO_2	2.609	3.381	3.076	2.919	3.457	3.272	3.501	3.632	3.291	3.350	2.808	3.435	3.670	2.348	2.896	2.276	3.088	3.472	3.222	3.287	3.137	3.377	3.162
ThO_2	10.540	13.150	11.733	11.262	14.023	12.587	15.471	14.811	13.142	13.570	10.602	12.991	13.840	10.037	11.223	8.902	12.450	14.214	13.231	13.583	12.651	13.876	13.337
UO_2	0.161	0.350	0.305	0.303	0.278	0.507	0.277	0.298	0.333	0.297	0.249	0.338	0.635	0.245	0.411	0.252	0.427	0.257	0.213	0.234	0.333	0.266	0.247
Al_2O_3	bd	bd	bd	bd	bd	bd	bd	bd	bd	bd	bd	bd	bd	bd	bd	bd	bd	bd	bd	bd	bd	bd	bd
Y_2O_3	0.491	0.266	0.269	0.283	0.199	0.878	0.703	0.281	1.384	0.514	0.807	0.287	0.524	0.787	0.341	0.224	0.318	0.211	0.239	0.220	0.440	0.238	0.729
La_2O_3	10.968	11.782	12.236	12.505	12.102	9.803	9.270	10.424	8.405	10.760	10.492	12.436	9.599	10.435	13.460	15.293	13.284	11.965	12.281	12.438	12.381	12.112	9.623
Ce_2O_3	27.775	27.740	28.533	28.705	28.409	25.462	25.459	26.253	24.173	27.653	27.096	28.729	26.041	27.323	30.025	31.070	29.433	28.617	28.594	28.624	28.173	28.562	26.291
Pr_2O_3	3.549	3.308	3.408	3.277	3.136	3.327	3.354	3.371	3.390	3.445	3.436	3.205	3.445	3.507	3.314	3.281	3.212	3.339	3.232	3.298	3.344	3.266	3.429
Nd_2O_3	12.508	11.261	11.192	10.684	10.087	12.634	12.377	11.737	13.288	11.352	11.976	10.181	12.119	12.790	10.074	9.603	10.032	10.654	10.695	10.555	11.086	10.488	12.453
Sm_2O_3	2.151	1.695	1.690	1.490	1.280	2.773	2.432	2.031	3.405	1.761	2.361	1.361	2.495	2.676	1.184	1.100	1.183	1.392	1.465	1.426	1.556	1.429	2.517
Eu_2O_3	bd	bd	bd	bd	bd	bd	bd	bd	bd	bd	bd	bd	bd	bd	bd	0.095	bd	bd	0.075	bd	bd	bd	bd
Gd_2O_3	1.004	0.699	0.707	0.559	0.345	1.457	1.142	0.817	1.831	0.710	1.152	0.503	1.231	1.342	0.500	0.326	0.501	0.489	0.541	0.453	0.653	0.478	1.157
Tb_2O_3	0.120	bd	bd	bd	bd	0.111	bd	bd	0.198	bd	0.177	bd	0.097	0.113	bd	bd	bd	bd	bd	bd	bd	bd	0.132
Dy_2O_3	0.283	0.179	0.222	0.157	0.154	0.610	0.364	0.233	0.762	0.202	0.517	0.209	0.517	0.521	0.173	0.107	0.118	0.136	0.185	0.162	0.213	0.120	0.452
Ho_2O_3	bd	bd	bd	bd	bd	0.119	bd	bd	bd	bd	bd	bd	bd	bd	bd	bd	bd	bd	bd	bd	bd	bd	bd
Er_2O_3	0.339	0.376	0.358	0.353	0.337	0.420	0.394	0.362	0.371	0.331	0.451	0.332	0.406	0.384	0.335	0.335	0.351	0.377	0.297	0.342	0.362	0.386	0.361
Tm_2O_3	0.107	bd	bd	0.077	bd	bd	bd	bd	bd	bd	0.091	0.099	bd	0.082	0.085	bd	0.075	bd	0.074	0.074	0.093	bd	bd
Yb_2O_3	0.150	0.128	0.136	0.154	0.165	0.168	0.133	0.108	0.203	0.138	0.144	0.129	0.172	0.132	0.154	0.149	0.116	0.133	0.133	0.144	0.125	0.138	0.155
Lu_2O_3	bd	0.104	0.106	bd	0.112	bd	0.132	bd	0.131	bd	0.141	0.109	bd	0.111	0.116	0.093	0.103	bd	bd	bd	bd	0.099	0.096
CaO	0.116	0.036	0.033	0.027	0.031	0.073	0.130	0.053	0.245	0.084	0.213	0.050	0.080	0.128	0.042	0.039	0.036	0.041	0.061	0.041	0.112	0.041	0.190
FeO	bd	bd	bd	bd	bd	bd	bd	bd	0.089	bd	1.561	0.148	bd	bd	bd	bd	bd	bd	bd	bd	bd	bd	bd
SrO	bd	bd	bd	bd	bd	bd	bd	bd	bd	bd	bd	bd	bd	bd	bd	bd	bd	bd	bd	bd	bd	bd	bd
PbO	0.140	0.178	0.166	0.155	0.189	0.169	0.201	0.197	0.178	0.175	0.160	0.186	0.196	0.136	0.160	0.119	0.183	0.183	0.176	0.180	0.173	0.179	0.177
Total	97.14	97.86	98.05	97.07	97.60	98.28	98.96	97.89	98.44	97.92	99.09	99.25	98.99	98.95	99.35	99.42	99.69	99.76	99.20	99.20	99.54	98.98	99.16
Age	306	300	314	306	304	285	294	299	298	289	*336*	317	296	303	308	298	318	293	304	303	303	292	301

bd – below detection limit

336 - ages not included in the age calculation

Table 2.
Electron microprobe analyses of twelve analyzed grains (wt%), continued.

Sample	AAR1																				
Grain	mz4						mz5					mz7				mz8					
Point no.	1	2	3	4	5	6	1	2	3	4	6	1	2	3	4	1	2	3	4	5	6
SO_3	bd	bd	0.026	bd	bd	bd	0.032	bd	bd	bd	bd	bd	bd	bd	bd	0.027	0.029	bd	bd	0.028	bd
P_2O_5	25.123	24.020	24.268	23.804	24.362	22.903	23.624	26.052	24.435	24.742	25.384	21.993	23.576	22.574	24.423	26.020	25.975	24.820	22.659	23.823	23.658
As_2O_5	0.260	0.285	0.266	0.267	0.231	0.281	0.259	0.296	0.264	0.291	0.287	0.260	0.257	0.284	0.273	0.266	0.277	0.275	0.243	0.276	0.294
SiO_2	2.634	3.110	3.044	2.917	2.945	3.619	3.547	1.883	2.654	2.815	2.431	4.039	2.988	3.507	2.767	2.572	2.111	2.332	3.774	2.957	3.169
ThO_2	9.843	15.092	12.517	11.976	11.232	14.843	13.140	7.343	11.019	11.999	10.404	13.885	11.548	11.792	11.034	10.150	8.951	9.652	15.642	12.677	11.588
UO_2	0.279	0.234	0.252	0.241	0.457	0.294	0.732	0.257	0.196	0.200	0.203	0.802	0.196	0.272	0.265	0.286	0.173	0.177	0.184	0.163	0.207
Al_2O_3	bd	bd	bd	bd	bd	bd	bd	bd	bd	bd	bd	bd	bd	0.049	bd	bd	bd	bd	bd	bd	0.002
Y_2O_3	0.395	0.319	0.549	0.517	0.262	0.538	0.544	0.764	0.852	0.816	0.844	0.774	0.256	0.394	0.528	0.534	0.861	0.827	0.496	0.721	0.546
La_2O_3	13.301	11.757	12.131	12.219	14.370	11.751	9.704	10.572	9.605	9.611	9.750	9.504	13.255	12.630	11.765	13.841	10.071	10.039	11.451	10.923	11.490
Ce_2O_3	28.732	27.398	28.521	28.763	29.939	27.509	26.595	28.144	26.391	26.079	26.845	24.918	29.158	28.022	28.057	30.439	27.409	27.074	26.259	26.439	28.167
Pr_2O_3	3.332	3.249	3.231	3.342	3.219	3.082	3.455	3.637	3.610	3.510	3.485	3.266	3.257	3.154	3.387	3.240	3.691	3.510	3.172	3.266	3.387
Nd_2O_3	11.534	11.111	10.570	10.446	9.487	10.066	11.718	13.647	13.135	12.917	13.265	12.110	10.312	9.799	11.499	9.582	13.504	13.053	11.055	11.785	11.225
Sm_2O_3	1.693	1.798	1.557	1.596	0.962	1.556	2.428	3.013	2.865	2.854	2.867	2.518	1.454	1.232	2.043	1.338	2.966	2.828	1.771	2.168	1.818
Eu_2O_3	bd	bd	bd	bd	bd	bd	bd	bd	bd	bd	bd	0.075	bd	bd	bd	bd	bd	bd	bd	bd	bd
Gd_2O_3	0.611	0.826	0.723	0.757	0.321	0.710	1.103	1.440	1.438	1.528	1.500	1.151	0.538	0.355	0.852	0.689	1.541	1.464	0.881	1.053	0.787
Tb_2O_3	bd	bd	bd	0.097	bd	bd	0.101	0.139	0.173	0.128	0.191	0.171	bd	bd	bd	bd	0.148	0.097	bd	bd	bd
Dy_2O_3	0.205	0.271	0.301	0.282	0.123	0.250	0.584	0.609	0.625	0.609	0.585	0.439	bd	bd	0.189	0.173	0.631	0.542	0.269	0.401	0.249
Ho_2O_3	bd	bd	bd	bd	bd	bd	bd	bd	bd	bd	bd	bd	bd	bd	bd	bd	bd	bd	bd	bd	bd
Er_2O_3	0.336	0.337	0.339	0.358	0.290	0.376	0.442	0.374	0.373	0.368	0.379	0.452	0.312	0.337	0.389	0.372	0.402	0.392	0.333	0.382	0.379
Tm_2O_3	0.087	bd	0.112	0.082	0.096	0.104	0.085	bd	bd	bd	0.087	bd	bd	bd	bd	0.070	0.078	bd	0.080	bd	0.072
Yb_2O_3	0.135	0.113	0.147	0.164	0.116	0.165	0.167	0.137	0.154	0.159	0.136	0.084	bd	bd	bd	0.465	0.474	0.435	0.498	0.480	0.463
Lu_2O_3	bd	bd	0.095	0.115	0.120	0.105	0.089	bd	0.121	0.130	bd	0.109	bd	0.145	0.114	0.103	0.107	bd	bd	bd	bd
CaO	0.072	0.121	0.096	0.084	0.047	0.095	0.105	0.113	0.194	0.204	0.220	0.085	0.089	0.094	0.141	0.089	0.230	0.258	0.156	0.234	0.173
FeO	bd	bd	bd	bd	bd	bd	bd	bd	bd	bd	bd	0.345	0.072	1.861	0.140	bd	bd	bd	bd	bd	0.362
SrO	bd	bd	bd	bd	bd	bd	bd	bd	bd	bd	bd	bd	bd	bd	bd	bd	bd	bd	bd	bd	0.036
PbO	0.134	0.193	0.165	0.155	0.154	0.191	0.192	0.099	0.144	0.156	0.142	0.199	0.149	0.186	0.151	0.144	0.115	0.126	0.202	0.160	0.154
Total	98.94	100.47	99.08	98.26	98.92	98.59	98.72	98.74	98.39	99.28	99.17	97.21	97.63	96.98	98.22	100.56	99.85	98.22	99.41	98.27	98.51
Age	303	292	297	293	293	290	297	295	297	297	309	290	296	*353*	305	313	293	296	298	291	302

bd – below detection limit

336 - ages not included in the age calculation

Table 2. Electron microprobe analyses of twelve analyzed grains (wt%), continued.

Sample	AAR1															AAR3					
Grain	mz9						mz10				mz1x					mz2					
Point no.	1	2	3	4	5	6	1	2	3	4	1	2	3	5	6	1	2	3	4	5	6
SO_3	0.026	bd	bd	bd	0.027	bd	bd	bd	bd	0.028	bd	bd	0.026	bd	0.027	bd	0.026	bd	bd	bd	bd
P_2O_5	24.344	25.066	24.976	26.245	26.280	24.432	25.038	24.425	23.779	25.152	24.359	23.850	24.032	24.694	24.431	23.453	23.455	23.731	24.437	22.190	22.393
As_2O_5	0.239	0.260	0.294	0.235	0.293	0.274	0.274	0.235	0.259	0.297	0.282	0.318	0.279	0.313	0.304	0.279	0.257	0.264	0.281	0.318	0.287
SiO_2	2.610	2.330	2.330	1.414	1.289	2.688	2.466	2.785	2.624	1.915	2.821	2.674	2.556	2.521	2.319	2.872	3.246	3.488	2.704	3.672	3.700
ThO_2	10.137	9.584	9.712	4.624	4.536	10.255	9.514	9.990	9.909	6.680	10.271	9.463	9.127	9.197	9.030	11.484	13.364	12.942	11.982	14.976	14.473
UO_2	0.350	0.209	0.207	0.135	0.119	0.374	0.391	0.389	0.300	0.209	0.322	0.302	0.252	0.309	0.258	0.148	0.215	0.535	0.196	0.241	0.246
Al_2O_3	bd	bd	bd	bd	bd	bd	bd	bd	0.019	0.031	bd	bd	bd	bd	bd	bd	bd	bd	bd	bd	bd
Y_2O_3	0.297	0.765	0.741	0.433	0.410	0.300	0.338	0.427	0.449	0.703	0.438	0.454	0.405	0.499	0.471	0.503	0.235	2.088	0.517	0.311	0.374
La_2O_3	14.193	10.671	10.798	12.785	12.962	13.889	14.234	13.377	13.019	10.715	10.674	10.908	11.090	10.522	11.148	11.399	11.980	8.111	10.192	11.156	11.021
Ce_2O_3	30.244	27.957	27.953	30.480	30.448	30.336	31.053	30.225	30.071	28.668	27.029	27.752	27.794	26.907	27.641	27.390	28.162	22.859	27.734	26.944	26.934
Pr_2O_3	3.278	3.516	3.558	3.756	3.728	3.326	3.283	3.202	3.357	3.556	3.660	3.750	3.609	3.771	3.682	3.237	3.224	3.344	3.508	3.307	3.218
Nd_2O_3	9.770	12.737	12.748	13.356	13.514	9.940	9.608	9.417	10.275	12.698	14.031	14.742	13.729	14.610	14.031	11.471	10.419	12.885	12.376	10.547	10.824
Sm_2O_3	1.120	2.531	2.603	2.153	2.210	1.062	1.064	1.252	1.401	2.857	2.087	2.141	1.969	2.216	2.131	1.947	1.522	3.452	2.222	1.590	1.676
Eu_2O_3	bd	bd	bd	bd	bd	bd	bd	bd	bd	bd	bd	bd	bd	bd	bd	bd	bd	bd	bd	bd	bd
Gd_2O_3	0.377	1.326	1.306	1.013	0.947	0.481	0.286	0.474	0.570	1.441	0.681	0.788	0.573	0.727	0.665	0.720	0.422	1.975	0.902	0.567	0.571
Tb_2O_3	bd	0.114	0.124	bd	bd	bd	bd	bd	bd	0.128	bd	bd	bd	bd	bd	bd	bd	0.212	bd	0.980	bd
Dy_2O_3	0.122	0.504	0.495	0.282	0.266	0.186	0.110	0.177	0.195	0.572	0.232	0.234	0.201	0.282	0.240	0.351	0.226	0.944	0.349	0.198	0.195
Ho_2O_3	bd	bd	bd	bd	bd	bd	bd	bd	0.109	0.100	bd	bd	bd	bd	bd	bd	bd	bd	bd	bd	bd
Er_2O_3	0.341	0.383	0.418	0.352	0.313	0.351	0.323	0.298	0.311	0.402	0.342	0.347	0.352	0.342	0.349	0.379	0.353	0.493	0.380	0.345	0.322
Tm_2O_3	bd	0.092	0.097	0.075	0.077	bd	0.055	0.092	bd	0.076	bd	0.085	bd	bd	bd	bd	bd	bd	bd	0.078	0.087
Yb_2O_3	0.147	0.132	0.118	0.112	0.134	0.108	0.120	0.096	0.147	0.182	0.128	0.132	0.165	0.129	0.117	0.135	0.139	0.196	0.116	0.131	0.171
Lu_2O_3	0.113	0.114	bd	bd	bd	0.106	bd	bd	bd	bd	bd	0.093	bd	bd	bd	bd	bd	0.110	bd	0.093	bd
CaO	0.044	0.169	0.155	0.082	0.047	0.043	0.086	0.107	0.101	0.307	0.070	0.075	0.091	0.088	0.066	0.162	0.046	0.121	0.125	0.062	0.083
FeO	bd	bd	bd	0.215	bd	bd	bd	0.045	bd	0.011	bd	bd	bd	bd	bd	0.022	bd	0.051	0.026	bd	bd
SrO	bd	bd	bd	bd	bd	bd	bd	bd	bd	bd	bd	bd	bd	bd	bd	bd	bd	bd	bd	bd	bd
PbO	0.135	0.126	0.128	0.065	0.063	0.147	0.132	0.147	0.127	0.090	0.143	0.129	0.133	0.132	0.125	0.158	0.172	0.182	0.160	0.195	0.193
Total	98.06	98.64	98.94	97.95	97.86	98.46	98.55	97.37	97.31	96.89	97.77	98.32	96.58	97.51	97.32	96.45	97.67	98.15	98.47	97.12	96.98
Age	291	296	297	318	317	309	297	316	284	300	304	300	324	312	306	318	294	295	305	298	304

bd – below detection limit

336 - ages not included in the age calculation

on binary diagrams (Poitrasson *et al*. 2000; Harlov *et al*. 2002; Williams *et al*. 2011; Seydoux-Guillaume *et al*. 2012). Unfortunately no measurement spots were located in thin BSE-dark domains near the cracks, so the nature of element depletion is unknown. However, as they were not included in the dating, their potential hydrothermal origin did not affect the age calculations. Taking into account both the compositional and textural characteristics of the grains, a magmatic origin is suggested for the entire population of monazites used for chemical dating. Places where fluid overprint is a possibility (cracks or lobate margins) either show a composition which is not significantly altered or were carefully avoided in the selection of the measurement spots.

Monazite ages

The monazite chemical dating yielded an uniform age of 299 ± 1.7 Ma (2σ) (Text-fig. 5ab) for the whole population. Single spot ages range from 281 Ma to 318 Ma. No systematic difference between the ages calculated for BSE-dark and BSE-bright zones of the entire monazite population can be observed. Both compositional domains demonstrate similar age distribution (289–318 Ma for BSE-ark zones and 291–318 Ma for BSE-bright zones). In single grains the ages calculated for BSE-dark zones are either younger or older from those calculated for BSE-bright, depending on the grain.

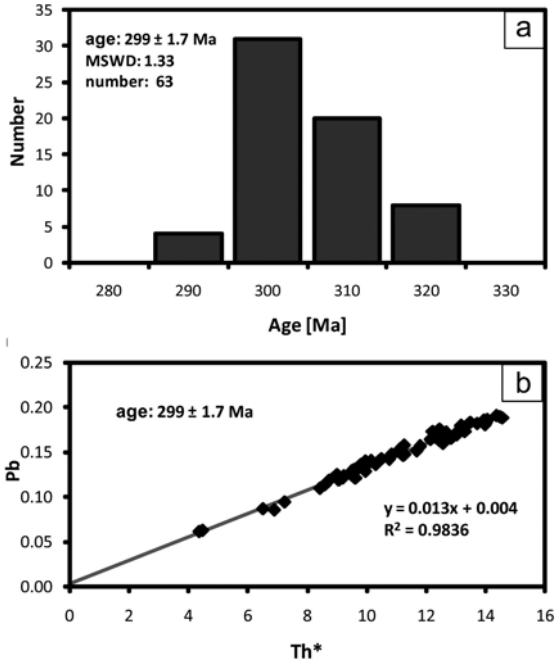

Text-fig. 5. Results of age calculation (with two abnormal ages substracted); a – histogram of monazite Th-U-Pb ages; b –total Pb vs. Th* (wt%) isochron diagram, where Th* is Th + U equivalents expressed as Th. Isochrons are calculated from regression forced through zero as proposed by Montel *et al.* (1996)

A systematic age difference between BSE-dark and BSE-bright zones might suggest an involvement of a secondary process affecting the monazite chemistry and, consequently, the ages obtained; however, no such feature is observed. In cases where BSE-dark zones might have originated from fluid infiltration (indicated by an irregular, lobate boundary of the margin), e.g. in grain AAR1-mz5, point 2 (Text-fig. 3g), the younger age of 295 Ma may be considered to be a result of selective leaching of Pb by F-bearing fluids (Williams *et al*. 2011), but no definite interpretation can be proposed based on only one analysis. In the case of grain AR-mz9, where the upper margin is depleted in Th, U and Pb, the age calculated for spots 4 and 5 is older than for the rest of the grain as well as the majority of measured points. Such case could be explained by fluid-aided removal of Th from the grain margin, but, as in the previous example, there is not sufficient evidence to confirm or exclude this suggestion. Selective leaching of Th, U or Pb by hydrothermal fluids may disturb the Th-U-Pb system and, therefore, yield an unrealistic age or even totally reset the Th-U-Pb clock (Bosse *et al*. 2009; Williams *et al*. 2011; Seydoux-Guillaume *et al*. 2012). The domains which are texturally suspected of being altered by post-magmatic fluids include BSE-dark cracks and some lobate grain margins. However, as mentioned above, compositional evidence of fluid-mediated alteration is scarce. As no measurement spots were located in the BSE-dark zones along the cracks, the potential disruption of the Th-U-Pb system by these domains was avoided. In the case of the margins, single examples show younger ages (e.g. AAR1-mz5, point 2). However, their number is insufficient to visibly disturb the age calculated for the whole population. Looking at textural, compositional and geochronological data, it can be stated that the studied monazite formed during one magmatic episode in a slightly heterogeneous magma and was moderately affected by post-magmatic fluids. Such an overlap of processes was already documented by the accessory mineral study of the Stolpen granite (Lisowiec *et al*. 2013). The selection of spots eliminated the effect of fluid alteration and thecalculated age can be treated as the magmatic age of monazite crystallization.

However meaningful the obtained age is (textural evidence, high precision and geotectonic context point to its high reliability), it must be stressed that electron microprobe dating of monazite is not the most precise dating method (compared to SHRIMP or TIMS). The age precision depends on the precision of the microprobe measurement itself and there is a number of analytical factors influencing the measurement error, such as counting statistics, background measurements, peak overlap corrections etc. (Pyle *et al*. 2005; Williams *et al*.

2006). Therefore the calculated age and its precision must be treated with caution.

Another important issue that must be taken into account when using minerals for dating is the stage at what the mineral appears during magmatic differentiation. Monazite usually starts to crystallize in the middle to late stages so that it records only exactly this time. As mentioned earlier, monazite occurs both as inclusions in either feldspar of fluorite and as large crystals in the rock matrix, which represent subsequent monazite generations. However, chemical dating was performed on heavy mineral separates, so the textural context of the studied monazite grains is lost. Nevertheless, it can be assumed that the separated monazite crystals (which are not intergrown with any other minerals) represent most probably the 'matrix' population, which is more prone to be released during crushing and heavy liquid separation. Consequently, this population reflects most likely the beginning of monazite crystallization. Therefore the age of 299 ± 1.7 Ma records the early stages of monazite formation. However, as monazite usually starts to crystallize in the middle to late stages of magma differentiation, the calculated age must be considered as a minimum age of the intrusion as granitoid plutons may form over wide time spans.

Variscan magmatism of Saxo-Thuringian zone of the Bohemian Massif

The monazite age is the first obtained for the Stolpen magmatic body. It confirms the previous suggestion that the Stolpen granite is one of the late-Variscan intrusions in the Lusatian Granodiorite Complex (Hammer *et al*. 1999). The magmatic activity started most probably earlier than the obtained age; as it lasted until at least 299 ± 1.7 Ma, the granite may be regarded as one of the youngest plutons in the whole intrusive sequence within the Saxo-Thuringian and Moldanubian zones. This information is particularly important for the determination of the whole path of evolution of the magmatism during the convergence of Gondwana and Laurussia (Matte 1986; Ziegler 1986; Finger and Steyrer 1990; Matte *et al*. 1990; Dallmeyer *et al*. 1995; Franke 2000; Franke *et al*. 2005). The Lusatian Complex belongs to the mid-European segment of the Variscan orogenic belt. The belt,which resulted from continent-continent collision, shows the emplacement of many granitic bodies (Finger *et al*. 1997). The greatest magmatic activity took place during the Late Carboniferous and was related to transpressional-transtensional tectonics (Finger and Steyrer 1990; Diot *et al*. 1995; Mazur and Aleksandrowski 2001). The plutons located at the northern extreme of the Bohemian Massif were emplaced during this period. They are all composite bodies of mixed mantle-crust origin (Gerdes *et al*. 2000; Janousek *et al*. 2004, Finger *et al*. 1997; Słaby and Martin 2008). Within these plutons, the Stolpen granite seems to present the final stage of a long lasting magmatism.

In general, two stages of granite emplacement within the Saxo-Thuringian and Moldanubian zones can be distinguished. Förster and Romer (2010) concluded that igneous activity in the Saxo-Thuringian Zone, including the northern and northwestern part of the Bohemian Massif, occurred at 335–320 Ma and 305–280 Ma. Some of the plutons, e.g. the granitoid pluton of Karkonosze, formed over several My, with the oldest rocks from this intrusion dated at 319–320 Ma (U-Pb in zircon, Žák *et al*. 2013), and the youngest at 302 ± 4 Ma (U-Pb in zircon, Kusiak *et al*. 2014). Finger *et al*. (2009) and Siebel *et al*. (2003) studied the Moldanubian part of the Bohemian Massif and also distinguished two major intrusive events; one more voluminous between 328–320 Ma, and the second one, less voluminous, between 317–310 Ma. Moreover, Finger *et al*. (2009) subdivided Variscan granitoid intrusions into five groups of granite belts characterized by slightly different ages, geotectonic settings and magma generation mechanisms. The oldest are: "North Variscan Granite Belt", "Central Bohemian Granite Belt" and "Durbachitic Granites", with ages of ca. 330 to 350 Ma, 360 to 335 Ma and 335 to 340 Ma, respectively. Intrusions with a younger age (330 to 310 Ma) include the south-western sector of the Bohemian Massif, and the granites from the western Erzgebirge and Fichtelgebirge. According to Finger *et al*. (2009) they form a coherent plutonic belt ("Saxo-Danubian Granitic Belt"), formed most probably due to the delamination of lithospheric mantle (Bird 1979). The fifth group, involving the youngest granites located in the Sudetes, is called the "Sudetic Granite Belt" (including e.g., Karkonosze Massif, Strzegom-Sobotka Massif, Strzelin Massif and Kłodzko-Złoty Stok Massif; Mazur *et al*. 2007) and is dated at ca. 315 to 300 Ma. Gerdes *et al*. (2003) reported a bimodal timing of magmatism in the South Bohemian Massif, with the first pulse at 331–323 Ma (with a higher mantle input) and the second, less significant, at 319–315 Ma. According to Siebel *et al*. (2010), one of the youngest magmatic impulses in the Bohemian Massif was the Fichtelgebirge intrusive complex, with U-Pb zircon ages ranging from 291.2 ± 6.4 Ma to 298.5 ± 3.9 Ma for different types of granites comprising the intrusion. Late-Variscan granitoids from the Erzgebirge fall within the older group of intrusions (Romer *et al*. 2010), whereas the younger magmatic event is absent. The ages of the amphibole-bearing granitoids

from the Lusatian Granodiorite Complex (granitoids from Wiesa – 304 ± 10 Ma and Klienschweidnitz – 312 ± 10 Ma) place these intrusions within the youngest stage of magmatic activity. The granite of Königshain was dated first by Hammer *et al*. (1999) at 315 ± 6 Ma using zircon-evaporation method and would also belong to the younger set of intrusions. However Th-U-total Pb dating of uraninite and molybdenite by Förster *et al*. (2012) yielded older ages of 328.6 ± 1.9 Ma for uraninite and 327 ± 1.3 Ma, 327.6 ± 1.3 Ma for molybdenite, indicating that the magmatic processes in the LGC started approximately at the same time as the older igneous events in other parts of the Saxo-Thuringian Zone and the Bohemian Massif. The granitoid pluton of Stolpen, with monazite age of 299 ± 1.7 Ma seems to be younger than its neighbour and belongs to the second impulse of magmatic activity in the Saxo-Thuringian Zone (Förster and Römer 2010). The age difference between the Stolpen and Königshain intrusions, which cannot be fully estimated based on present data, is difficult to explain, especially as these two plutons are located in one geotectonic unit. It is possible that the studied samples were taken from the youngest part of the pluton, whereas the main body formed some million years before. Nevertheless the Stolpen granite, or at least part of it, is the youngest intrusion in the Lusatian Granodiorite Complex, indicating that the magmatic activity in this region lasted at least 5 my longer than previously estimated.

According to previous studies of the biotite-bearing granitoid intrusions from the Lusatian Granodiorite Complex, magma generation mechanisms involved melting of the lower crust triggered by a mantle diapir (enriching the granitoid rocks in LILE and HFSE), accompanied by post-collisional extension (Hammer *et al*. 1999) in the case of the Stolpen granite, and crust melting in a compressional regime in case of the Königshain granite (Eidam *et al*. 1991). Amphibole-bearing granitoids (from Wiesa and Kleinschweidnitz) formed due to melting of metasomatized mafic lower crust (probably tholeiitic, Hammer *et al*. 1999). The melting of the lower crust, in the case of both biotite- and amphibole-bearing granites, was induced probably by delamination processes, as proposed by Hammer *et al*. (1999). A similar scenario for the Late Carboniferous – Early Permian magmatism in Central Europe is also suggested by more recent studies of Finger *et al*. (2009), Słaby *et al*. (2010) and Turniak *et al*. (2014). Finger *et al*. (2009) proposed a delamination model for the formation of the Saxo-Danubian granitoids, which extend along the NE and SW margins of the Bohemian Massif. Late Variscan Lusatian granitoids (including Stolpen) may be considered as the most northerly part of this belt, but the younger age of the Stolpen granite is not in accord with the older rocks formed south-west of the pluton (e.g. in the Erzgebirge). Studies of the Strzegom–Sobotka Massif (Turniak *et al*. 2014) belonging to the Sudetic Granitic Belt, have suggested a close relationship to post-Variscan bimodal volcanism. The heat required for melting of the lower crust was supplied by the ascent of mantle-derived basaltic magmas. The mechanisms possibly responsible for melting of the lithospheric mantle include decompression related to lithospheric extension/rifting and delamination and the convective removal of the thickened mantle. Perhaps similar mechanisms operated in the LGC, which is a western prolongation of the Sudetic Granitic Belt. An interesting comparison can be also made with the granitic rocks (dated at ~300 Ma) associated with the Kraków-Lubliniec Fault Zone (located to the East of the Variscides) which is a prolongation of the Elbe Line (near which the Stolpen granite is located). Słaby *et al*. (2010) proposed a two-stage origin, involving: (1) transpressional regime accompanied by crustal thickening, delamination of the lithospheric mantle and mantle metasomatism , and (2) transtensional regime causing partial melting of upper metasomatized mantle and lower mafic crust. Therefore, it seems that similar processes may have caused granitoid formation along the Elbe Zone and its extension to the Kraków-Lubliniec Fault Zone. The age of the Stolpen granite agrees with such an assumption.

Magmatism in the Bohemian Massif is characterized by magmas derived from at least two sources: mantle and crust (Finger *et al*. 1997; Janousek *et al*. 2004; Gerdes *et al*. 2000; Siebel *et al*. 2003; Słaby and Martin 2008). It is noticeable that with progressive evolution of the magmatism, the contribution of the mantle source diminished and the peraluminosity of magmas increased. However mantle activity did not disappear entirely; it is present in a form of late mafic dykes. The Mantle source also contributed continuously with fluids, whose signature is discernible in the granite alterations products and granite pegmatites (e.g. Martin 2006), as is also seen in the case of the Stolpen granite (Lisowiec *et al*. 2013). The delamination scenario supports mantle-crust interactions, which may involve mixing between crust- and mantle-derived melts (as suggested for some granites from the Saxo-Danubian Granitic Belt, Finger *et al*. 2009) or can be limited to heat transfer and influx of mantle-derived fluids.

The Stolpen granite fits the general features of magma evolution in the Bohemian Massif. Both the obtained monazite age and magma affinity fit to the late stage of Variscan magmatism outline. The peraluminous character of the Stolpen granite and the only slight contribution of mantle fluids (Hammer *et al*. 1999; Lisowiec

et al. 2013) suggest that at the end of the emplacement of Variscan granitoids the interaction between the mantle and the crust was limited, but noticeable. The tectonic setting of the Stolpen pluton near the Stolpen-Klotzsche Fault indicates that the mechanism of emplacement along older shear zones was similar to those of other granites from the LGC, as e.g., the Königshain granite (Förster *et al*. 2012).

CONCLUSIONS

Chemical dating results of monazite point to a crystallization age related to the late magmatic stages of the formation of the Stolpen granite. Although textural data point to some weak secondary alteration present in the monazite grains, domains and spots for analysis were chosen so as to minimize the contribution of fluid-induced components. Chemical composition and dating results of the analyzed domains do not indicate post-magmatic processes.

The Th-U-total Pb monazite age of 299 ± 1.7 Ma indicates that the Stolpen granite is the youngest late Variscan intrusion present in the Lusatian Granodiorite Complex and one of the youngest of the Variscan granitic bodies in the Saxo-Thuringian Zone and the Bohemian Massif. It suggests that shear zones created during the Variscan Orogenesis in the LGC were still active at that time and enabled the emplacement of the granitic magma in upper parts of the crust. The young age of the granite and its location may suggest some affinity to other aspects of Late Carboniferous – Early Permian magmatism of Central Europe that formed due to lithospheric mantle-crust interactions in a changeable transpressional-transtensional regime and the following magmatic flare-up. Therefore, a similar magma generation mechanism can be proposed for the Stolpen granite;however such assumption remains only a hypothesis, which must be verified by further studies.

This study reports the first precise geochronological data on the Stolpen Granite and allows a better understanding of the evolution of the late Variscan magmatism in the LGC and in the whole Bohemian Massif.

Acknowledgements

We want to thank Patrik Konečný and the staff of the Department of Electron Microanalysis, State Geological Institute of Dionýz Štúr in Bratislava for the careful and professional analysis of the samples and calculation of the results. We also acknowledge Daniel Harlov for his helpful discussion of the results. Igor Broska and Ray MacDonald, are thanked for insightful reviews, and Ray MacDonald also for linguistic corrections of the final version. This study was funded by a NCN grant 2011/01/N/ST10/04756.

REFERENCES

Bird, P. 1979. Continental delamination and the Colorado Plateau. *Journal of Geophysical Research*, **84**, 7561–7571.

Cherniak, D.J. and Pyle, J.M. 2008. Th diffusion in monazite. *Chemical Geology*, **256**, 52–61.

Cherniak, D.J., Watson, E.B., Grove, M. and Harrison, T.M. 2004a. Pb diffusion in monazite: A combined RBS/SIMS study. *Geochimica Cosmochimica Acta*, **68**, 829–840.

Cherniak, D.J., Zhang, X.Y., Nakamura, M. and Watson, E.B. 2004b. Oxygen diffusion in monazite. *Earth and Planetary Science Letters*, **226**, 161–174.

Dallmeyer, R.D., Franke, W. and Weber, K.E.B. 1995. Pre-Permian geology of Central and Eastern Europe, pp. 1–604, Springer, Berlin.

Diot, H., Masur, S. and Pin, C. 1995. Karkonosze batolith (NE Bohemian Massif): The evidence for pluton emplacement during transtensional-extensional collapse. *Journal of Czech Geological Society*, **40**, 62.

Duthou, J.L., Couturié, J. P., Mierzejewski, M. P. and Pin, C. 1991. Rb/Sr age of the Karkonosze granite on the base of the whole rock method. *Przeglad Geologiczny,* **2**, 75–79.

Eidam, J. and Götze, J., 1991. The Granitic Massif of Königshain-Arnsdorf (Lusatian Anticlinal Zone). *Chemie der Erde,* **51**, 55–71.

Finger, F., Roberts, M.P., Haunschmid, B., Schermaier, A. and Steyrer, H.P. 1997. Variscan granitoids of central Europe: their typology, potential sources and tectonothermal relations. *Mineralogy and Petrology*, **61**, 67–96.

Finger, F. and Steyrer, H. P. 1990. I-Type Granitoids as Indicators of a Late Paleozoic Convergent Ocean-Continent Margin Along the Southern Flank of the Central-European Variscan Orogen. *Geology*, **18**, 1207–1210.

Finger, F. and Krenn, E. 2007. Three metamorphic monazite generations in a high-pressure rock from the Bohemian Massif and the potentially important role of apatite in stimulating polyphase monazite growth along a PT loop. *Lithos*, **95**, 103-115.

Finger, F., Gerdes, A., Rene, M., Riegler, G. 2009. The Saxo-Danubian Granite Belt: magmatic response to post-collisional delamination of mantle lithosphere below the southwestern sector of the Bohemian Massif (Variscan orogen). *Geologica Carpathica*, **60**, 205–212.

Förster, H.-J. and Romer, R.L. 2010. Carboniferous magmatism. In Linnemann, U. and Romer, R.L. (Eds), Pre-Mesozoic Geology of Saxo-Thuringia – From the Cadomian

Active Margin to the Variscan Orogen, pp. 287–308. Schweizerbart; Stuttgart.

Forster, H.J., Rhede, D., Stein, H.-J., Romer, R.L. and Tischendorf, G. 2012. Paired uraninite and molybdenite dating of the Konigshain granite: implications for the onset of late-Variscan magmatism in the Lausitz Block. *International Journal of Earth Sciences*, **101**, 57–67.

Franke, W. 2000. The mid-European segment of the Variscides: tectonostratigraphic units, terrane boundaries and plate tectonic evolution. In: Franke, W., Haak, V., Oncken, O., Tanner, D. (Eds), Orogenic Processes: Quantification and Modelling in the Variscan Belt. *Geological Society, London, Special Publications*, **179**, 35–61.

Franke, W., Matte, P., Tait, J. 2005. Europe; Variscan Orogeny. In: Encyclopedia of Geology, **2**, pp. 75–86. Elsevier; Oxford.

Gerdes, A., Wörner, G. and Finger, F. 2000. Hybrids, magma mixing and enriched mantle melts in post- collisional Variscan granitoids: the Rastenberg Pluton, Austria. In: W. Franke, V. Haak, O. Oncken and D. Tanner (Eds), Orogenic Processes: Quantification and Modelling in the Variscan Belt, *Geological Society Special Publication,* **179**, 415–431.

Gerdes, A., Friedl, G., Parrish, R.R. and Finger, F. 2003. High-resolution geochronology of Variscan granite emplacement - the South Bohemian Batholith. Journal of Czech Geological Society, **48**, 1–2.

Hammer, J., Eidam, J., Röber, R. and Ehling, B.C. 1999. Prävariszischer Und variszischer granitoider Magmatismus am NE-Rand des Böhmischen Massivs - Geochemie und Petrogenese. *Zeitschrift für Geologischen Wissenschaften*, **27**, 401–415.

Harlov, D., Förster, H.-J. and Nijland, T. G. 2002. Fluid-induced nucleation of (Y + REE)-phosphate minerals within apatite: Nature and experiment. Part I. Chlorapatite. *American Mineralogist*, **87**, 245–261.

Harlov, D., Wirth, R. and Hetherington, C. L. 2011. Fluid-mediated partial alteration in monazite: the role of coupled dissolution–reprecipitation in element redistribution and mass transfer. *Contributions to Mineralogy and Petrology*, **162**, 329–348.

Janousek,V., Braithwaite, C.J.R., Bowes, D.R. and Gerdes, A. 2004. Magma-mixing in the genesis of Hercynian calc-alkaline granitoids: an integrated petrographic and geochemical study of the Sazava intrusion, Central Bohemian Pluton, Czech Republic. *Lithos*, **78**, 67–99.

Jercinovic, M.J. and Williams, M.L. 2005. Analytical perils (and progress) in electron microprobe trace element analysis applied to geochronology: Background acquisition, interferences, and beam irradiation effects. *American Mineralogist*, **90**, 526–546.

Jercinovic, M.J., Williams, M.L. and Lane, E.D. 2008. In-situ trace element analysis of monazite and other fine-grained accessory minerals by EPMA. *Chemical Geology*, **254**, 197–215.

Just, J., Schulz, B., de Wall, H., Jourdan, F. and Pandit, M.K. 2011. Monazite CHIME/EPMA dating of Erinpura granitoid deformation: Implications for Neoproterozoic tectono-thermal evolution of NW India. *Gondwana Research*, **19**, 402–412.

Klein, T., Kiehm, S., Siebel, W., Shang, C.K., Rohrmüller, J., Dörr, W. and Zulauf, G. 2008. Age and emplacement of late-Variscan granites of the western Bohemian Massif with main focus on the Hauzenberg granitoids (European Variscides, Germany). *Lithos*, **102**, 478–507.

Kohn, M.J., Wieland, M.S., Parkinson, C.D. and Upreti, B.N. 2005. Five generations of monazite in Langtang gneisses: implications for chronology of the Himalayan metamorphic core. *Journal of Metamorphic Geology*, **23**, 399–406.

Konečný, P. 2004. Methodics of monazite dating using electron microprobe. *Mineralogia Slovakia*, **36**, 225–235.

Kozdrój, W., Krentz, O. and Opletal, M. (Eds) 2001. Geological map and Comments on the Geological Map Lausitz, Jizera, Karkonosze (without Cenozoic sediments) 1 : 100 000. Państwowy Instytut Geologiczny, Warsaw.

Kröner, A., Hegner, E., Hammer, J., Haase, G., Bielicki, K.-H., Krauss, M. and Eidam, J. 1994. Geochronology and Nd-Sr systematics of Lusatian granites: significance for the evolution of the Variscan orogen in east-central Europe. *Geologische Rundschau*, **83**, 357–376.

Kryza, R., Crowley, Q.D., Larionov, A., Pin, C., Oberc-Dziedzic, T. and Mochnacka, K. 2012. Chemical abrasion applied to SHRIMP zircon geochronology: An example from the Variscan Karkonosze Granite (Sudeted, SW Poland). *Gondwana Research*, **21**, 757–767.

Lisowiec, K., Budzyń, B., Słaby, E., Renno, A.D. and Götze, J. 2012. Fluid-induced magmatic and post-magmatic zircon and monazite patterns in granitoid pluton and related rhyolitic bodies. *Chemie der Erde*, **73**, 163–179.

Liu, Y., Siebel, W., Massonne, H.J. and Xiao, X.C. 2007. Geochronological and petrological constraints for tectonic evolution of the central Greater Himalayan Sequence in the Kharta area, southern Tibet. *Journal of Geology*, **115**, 215–230.

Marheine, D., Kachlik,V., Maluski, H., Patocka, F. and Zelazniewicz, A. 2002. The 40Ar/39Ar ages from the West Sudetes (NE Bohemian Massif): constraints on the Variscan polyphase tectonothermal development. In: Winchester, J.A., Pharaoh, T. and Verniers, J. (Eds), Palaezoic Amalgamation of Central Europe. *Geological Society, London, Special Publications*, **201**, 133–155.

Martin, R.F. 2006. A-type granites of crustal origin ultimately result from open-system fenitization-type reactions in an extensional environment. *Lithos*, **91**, 125–136.

Matte, P. 1986. Tectonics and Plate-Tectonics Model for the

Variscan Belt of Europe. *Tectonophysics*, **126**, 329–374.

Matte, P., Maluski, H., Rajlich, P. and Franke, W. 1990. Terrane Boundaries in the Bohemian Massif - Result of Large-Scale Variscan Shearing. *Tectonophysics*, **177**, 151–170.

Mazur, S. and Aleksandrowski, P. 2001. The Tepla(?)/ Saxothuringian suture in the Karkonosze-Izera Massif, western Sudetes, Central European Variscides. *International Journal of Earth Sciences*, **9**, 341–360.

Mazur, S., Aleksandrowski, P., Turniak, K. and Awdankiewicz, M, 2007. Geology, tectonic evolution and Late Paeleozoic magmatism of Sudetes – an overview. *Granitoids in Poland, AM Monograph*, **1**, 59–87.

Montel, J.M., Foret, S., Veschambre, M., Nicollet, C. and Provost, A. 1996. Electron microprobe dating of monazite. *Chemical Geology*, **131**, 37–53.

Oberc-Dziedzic, T., Kryza, R., Pin, C. and Madej, S. 2013. Variscan granitoid plutonism in the Strzelin Massif (SW Poland): petrology and age of the composite Strzelin granite intrusion. *Geology Quarterly*, **57**, 269–288.

Parrish, R.R. 1990. U-Pb Dating of Monazite and Its Application to Geological Problems. *Canadian Journal of Earth Sciences*, **27**, 1431–1450.

Poitrasson, F., Chenery, S. and Shepherd, T. J. 2000. Electron microprobe and LA-ICP-MS study of monazite hydrothermal alteration: Implications for U-Th-Pb geochronology and nuclear ceramics. *Geochimica Cosmochimica Acta*, **64**, 3283–3297.

Pyle, J.M., Spear, F.S., Wark, D.A., Daniel, C.G. and Storm, L.C. 2005. Contributions to precision and accuracy of monazite microprobe ages. *American Mineralogist*, **90**, 547–577.

Romer, R. L., Förster, H.-J. and Stemprok, M. 2010. Age constraints for the late-Variscan magmatism in the Altenberg-Teplice Caldera (Eastern Erzgebirge/Krusne hory). *Neues Jahrbuch für Mineralogie – Abhandlungen*, **187**, 289–305.

Rosa-Costa, L.T., Lafon, J.M., Cocherie, A. and Delor, C. 2008. Electron microprobe U–Th–Pb monazite dating of the Transamazonian high-grade metamorphic overprint on Archean rocks from Amapá Block, southeastern Guiana Shield, northern Brazil. *Journal of South American Earth Sciences*, **26**, 445–462.

Seydoux-Guillaume, A.-M., Montel, J.-M., Bingen, B., Bosse, V., de Parvesal, P., Paquette, J.-L., Janots, E. and Wirth, R. 2012. Low-temperature alteration of monazite: Fluid mediated coupled dissolution–precipitation, irradiation damage, and disturbance of the U–Pb and Th–Pb chronometers. *Chemical Geology*, **330-331**, 140–158.

Siebel, W., Chen, F. and Satir, M. 2003. Late-Variscan magmatism revisited: new implications from Pb-evaporation zircon ages on the emplacement of redwitzites and granites in NE Bavaria. *International Journal of Earth Sciences*, **92**, 36–53.

Siebel, W., Shang, C. K. and Presser, V. 2010. Permo-Carboniferous magmatism in the Fichtelgebirge: dating the final intrusive pulse by U-Pb, 207Pb/206Pb and 40Ar/39Ar geochronology. *Zeitschrift für Geologischen Wissenschaften*, **38**, 85−98.

Słaby, E. and Martin, H. 2008. Mafic and felsic magma interaction in granites: The Hercynian Karkonosze Pluton (Sudetes, Bohemian Massif). *Journal of Petrology*, **49**, 353–391.

Słaby, E., Breitkreuz, C., Żaba, J., Domańska-Siuda, J., Gaidzik, K., Falenty, K. and Falenty A. 2010. Magma generation in an alternating transtensional–transpressional regime, the Kraków–Lubliniec Fault Zone, Poland. *Lithos*, **119**, 251–268.

Spear, F.S., Pyle, J.M. and Cherniak, D. 2009. Limitations of chemical dating of monazite. *Chemical Geology*, **266**, 218–230.

Suzuki, K. and Adachi, M. 1991. Precambrian Provenance and Silurian Metamorphism of the Tsubonosawa Paragneiss in the South Kitakami Terrane, Northeast Japan, Revealed by the Chemical Th-U-Total Pb Isochron Ages of Monazite, Zircon and Xenotime. *Geochemical Journal*, **25**, 357–376.

Suzuki, K. and Adachi, M. 1994. Middle Precambrian Detrital Monazite and Zircon from the Hida Gneiss on Oki-Dogo Island, Japan – Their Origin and Implications for the Correlation of Basement Gneiss of Southwest Japan and Korea. *Tectonophysics*, **235**, 277–292.

Suzuki, K. and Kato, T. 2008. CHIME dating of monazite, xenotime, zircon and polycrase: Protocol, pitfalls and chemical criterion of possibly discordant age data. *Gondwana Research*, **14**, 569–586.

Tickyj, H., Hartmann, L.A., Vasconcellos, M.A.Z., Philipp, R.P. and Remus, M.V.D. 2004. Electron microprobe dating of monazite substantiates ages of major geological events in the southern Brazilian shield. *Journal of South American Earth Sciences,* **16**, 699–713.

Turniak, K., Mazur, S., Domańska-Siuda, J. and Szuszkiewicz, A. 2014. SHRIMP U-Pb zircon dating for granitoids from the Strzegom - Sobótka Massif, SW Poland: Constraints on the initial time of Permo-Mesozoic lithosphere thinning beneath Central Europe. *Lithos*, in print.

Williams, M.L., Jercinovic, M.J., Goncalves, P. and Mahan, K.H. 2006. Format and philosophy for collecting, compiling, and reporting microprobe monazite ages. *Chemical Geology*, **225**, 1–15.

Williams, M.L., Jercinovic, M.J. and Hetherington, C.J. 2007. Microprobe monazite geochronology: Understanding geologic processes by integrating composition and chronology. *Annual Reviews of Earth and Planetary Sciences*, **35**, 137–175.

Williams, M.L., Jercinovic, M.J., Harlov, D., Budzyn, B. and Hetherington, C.J. 2011. Resetting monazite ages during fluid-related alteration. *Chemical Geology*, **283**, 218–225.

Ziegler, P.A. 1986. Geodynamic Model for the Paleozoic Crustal Consolidation of Western and Central-Europe. *Tectonophysics*, **126**, 303–328.

Manuscript submitted: 20th January 2014
Revised version accepted: 15th September 2014